Multi-Temporal Inundated Areas Monitoring Made Easy: The Case of Kerkini Lake in Greece

Ioannis Manakos[1] [a], Malak Kanj[2] [b], Michail Sismanis[1] [c], Ioannis Tsolaikidis[3] [d]
and Chariton Kalaitzidis[2] [e]

[1]*Information Technologies Institute, Centre for Research and Technology Hellas, Thessaloniki, Greece*
[2]*Department of Geoinformation in Environmental Management, Mediterranean Agronomic Institute of Chania, Chania, Greece*
[3]*Lake Kerkini Management Authority, Kerkini, Serres, Greece*

Abstract: Satellite data may support management of wetland areas for monitoring of the inundation seasonality. Previously successful in Doñana and Camargue Biosphere Reserves, this study examines the transferability of unsupervised inundation mapping through automatic local thresholding in discriminating inundated areas from non-inundated ones in Kerkini Lake. Nine different alternatives of this approach are employed on Sentinel-2 (S2) Level-2A images (2016-2019). The best fit alternative was derived by the validation against local and on-site registered attributes. To overcome unfavourable atmospheric conditions, Sentinel-1 (S1) images were examined in tandem with derived S2 inundation maps (S2m), using the best fit alternative. Two S2m, one preceding and one following a target S1 image, were used to train random forest models (per pixel) to be applied to the target S1 image and derive the respective inundation map (S1m). S1m was validated against a S2m for the same date; not previously used in the training process. Classification performance reached k [0.77-0.94] and overall accuracy [88.05-97.16%] for the S2m. The evaluation of S1m showed k of 0.99 and overall accuracy between 99.71-99.88%. Automation of the process and minimum human interference supports its usage by non-specialists, e.g. for Protected Areas management.

1 INTRODUCTION

Wetlands are fundamental for maintaining life on Earth and demonstrate high biodiversity. They provide different ecosystem services that ultimately affect human wellbeing (Finlayson & D'Cruz, 2010; Millennium Ecosystem Assessment, 2005). They provide for food and shelter, flood control and climate regulation, as well as for supporting and maintaining biogeochemical cycles and soil formation. Nowadays, they are seen as having a cultural role to visitors, too, as they provide a good source of income from tourism and recreation. These ecosystem services along with their rapid decline as a result of human pressures and climate change urge for capacity improvement in monitoring status. In this context, water presence and extent across time is as seriously treated as water quality maintenance. The variability of water extent is vital for any decision to tackle any misbalances in ecosystem services (e.g. cattle feeding vs. bird nesting). Spaceborne Earth Observation monitoring can be a powerful approach for accurate and cost-effecting frequent monitoring of open water surfaces.

Numerous approaches, utilizing optical and radar data for water surface area estimation, can be used to rapidly generate flood extent maps in real time, with no additional need for supplementary data (Cohen et al., 2019; Marti-Cardona et al.,

[a] https://orcid.org/0000-0001-6833-294X
[b] https://orcid.org/0000-0002-6776-4692
[c] https://orcid.org/0000-0001-6387-5849
[d] https://orcid.org/0000-0001-6848-189X
[e] https://orcid.org/0000-0001-5217-7164

2013). Radar data-based approaches have an advantage over optical data ones by operating under nearly all weather and day-night conditions. However, emergent vegetation, waves, sand, and radar shadows produced by terrain features hinder the efficient delineation between water and land (Kordelas et al., 2019; Manakos et al., 2019). Evidently, extraction of the water surface from optical imagery is generally more straightforward than radar imagery. The rich spectral information of optical data allows for the reliable detection of the water presence by utilizing various indices and bands; especially, when applying thresholds to them. Commonly used thresholding approaches to indices, include Normalized Difference Water Index (NDWI) (Du et al., 2016; McFeeters, 1996; Zhang et al., 2018), Modified NDWI (Xu, 2006), and the Automated Water Extraction Index (Feyisa et al., 2014; Guo et al., 2017; Rokni et al., 2014; Zhang et al., 2018). Numerous classification methods, supervised and unsupervised, have been applied in detecting water bodies and their extent from multispectral imagery (Kordelas et al., 2019; Thenkabail, 2015). Furthermore, machine learning algorithms (MLA) have been employed for remote sensing image analysis and demonstrated improved accuracies for inundation map derivation. Commonly used MLAs include k-Means (Yousefi et al., 2018), Artificial Neural Networks (Skakun, 2010), Support Vector Machine (Nandi et al., 2017; Sarp & Ozcelik, 2017), Decision Trees (Acharya et al., 2019), and Random Forest (Feng et al., 2015; Ko et al., 2015). These classification-based approaches may achieve higher accuracy than thresholding; however, ground truth data are required to select appropriate training samples. This, in turn, requires skilled personnel or enhanced human interference with the process.

Focusing on non-supervised inundation mapping, automatic local thresholding methods have been successfully applied to Doñana and Camargue Biosphere Reserves; both with optical data alone or by fusing radar and optical data sources by means of machine learning, to increase information retrieval capacity (Kordelas et al. 2018, 2019; Manakos et al, 2019). This study examines the transferability of the methods to monitor inundation seasonality of a river deltaic system entering an inland lake at the foothills of Kerkini Mountain in North Greece.

2 MATERIALS AND METHODS

2.1 Study Area

Lake Kerkini (41°13'N, 23°08'E) refers to the artificial lake (reservoir) created in 1932 and the surrounding wetland area. Its surface area of 70-76 km^2 lies at the transboundary of Strymonas River in northern Greece close to the border with Bulgaria. Its drainage area extends over 11,600km^2, with the Hellenic sub-basin making up to 803 km^2 (Ovakoglou et al., 2016; Psilovikos & Margoni, 2010). Kerkini climate is an intermediate between Mediterranean and Mid-European, with hot summers and cold winters. The average annual rainfall reaches 463.5 mm and occurs in two peaks, one during the cold period of the year and the other during May-June (Gerakes, 1989).

Lake Kerkini has developed into one of the most popular stops for migratory bird populations in Europe, as well a wetland of international significance; established as a Natura2000 protected area and a RAMSAR wetland of international importance. Kerkini accommodates over 300 bird species; with at least 1300 plant species; including indigenous and rare species, as well as Greece's largest water buffalo population (*Bubalus bubalis*). Thus, understanding inundation seasonality is crucial for the Lake Kerkini Management Authority to balance nesting and feeding needs of the migrating birds, feeding needs of buffalos and irrigation needs of the Serres plain.

2.2 Satellite Imagery

Sentinel-2 Level-2A (L2A) products were downloaded from the Copernicus European Space Agency (ESA) hub between 6 September 2017 and 27 August 2019 (52 products), as well as 24 S2 Level-1C (L1C) products between 16 November 2015 and 23 July 2017. The acquired products comprise the tile 34TFL. S2 L1C Top-of-Atmosphere (TOA) products were processed to L2A Bottom-of-Atmosphere (BOA) products using Sentinel-2 Level2A Prototype Processor (Sen2Cor) software downloaded in the ESA SNAP Desktop third-party plugin of the Sentinel-2 Toolbox. Sen2Cor has a high performance in generating the Scene Classification layer (SCL) (92 ± 4%) (Main-Knorn et al., 2017).

To assess the application of the unsupervised automatic local thresholding during unfavourable atmospheric conditions for S2 image acquisition 11 S1 Ground Range Detected (GRD) images were

downloaded from the Copernicus Open Access Hub for the periods between 24 February 2019 to 26 March 2019 and 30 July 2019 to 29 August 2019. ESA SNAP was used for preprocessing the Sentinel-1 GRD using the command line graph processing framework, to (i) apply orbit file, (ii) remove thermal and border noise, (iii) calibration, (iv) speckle filtering using Lee Signa filter with a window-size of 5x5, (v) Range-Doppler Terrain Correction. The unitless backscatter coefficient is converted then to dB using a logarithmic transformation (Filipponi, 2019).

2.3 Validation Data

Acquisition dates (22 dates) coinciding with recurring water level measurements (2017-2019), provided by the Lake Kerkini Management Authority, are considered in the unsupervised inundation mapping by automatic local thresholding. Validation maps were delineated taking into consideration actual water level measurements (10-minute interval), bathymetry map with 10-m pixel resolution (Tsolakidis & Vafiadis, 2019), water class derived from the Copernicus SCL and expert local knowledge about the maximum expected annual fluctuation across decades. Specifically, in situ water level gauge measurements were combined with the bathymetry map (i.e. all pixels under the gauge level in the bathymetry map without barriers in-between are considered inundated). Then the expert knowledge across decades for the maximum flood elevation level ever reached was superimposed. In addition, information from the water class of the SCL was considered at positions, where sedimentation of the delta might have influenced information derived from existing but older bathymetry map.

2.4 Methodology

2.4.1 Local Automatic Thresholding of Sentinel-2

The work presented by Kordelas et al. (2018, 2019) introduced unsupervised approach in discriminating between inundated and non-inundated areas, through detecting automatic thresholds. The pre-processed S2 L2A image is segmented into non-overlapping regions to select segments with high percentage of inundated pixels. Then an expanding patch based approach, taking into consideration medians of percentages of inundated/ non inundated areas, is followed based on the centroids of the segments.

The open water subclass is examined by estimating the initial threshold with the ability to separate inundated pixels from non-inundated ones through the use of: (i) SWIR-1 Band (Alt1), (ii) product of SWIR-2 and NIR (Alt2) and (iii) product of SWIR-1 and NIR (Alt3). The initial threshold is calculated as the first deep valley the histogram can detect. The final threshold is calculated based on (i) the minimum cross entropy thresholding algorithm (MCET), (ii) Otsu's algorithm or (iii) the average between them, resulting in nine different alternatives from all possible combinations of data and thresholding method taken into consideration. The performance of each of the alternatives is assessed by its ability to accurately distinguish between inundated and non-inundated pixels, against the validation data, using the overall accuracy of the validation dates and the overall Kappa coefficients (Congalton & Green, 2009; Whitten et al., 2011).

2.4.2 Pixel-centric Classification of Sentinel-1

Under the unavailability of data or unfavourable weather conditions S2m cannot be generated, hence, producing a gap in the monitoring capacity. To counterbalance this, Manakos et al. (2019) proposed the use of multiple local random forest classifiers' estimation per pixel, based on S1 images timely close or coinciding with S2m dates. The training set is created for 3x3 pixel samples, with the features being the pixel's backscatter coefficients for bands VH and VV, algebraic combinations of the same bands, and the season of the year, while the reference class for each pixel is derived from the closest S2m. Pixel-centric classification is performed on the S1 target date data using the trained classifiers, based on the location in the image, to delineate the required inundation map (S1m). The method used in this work is abbreviated as TIM (after Manakos et al. (2019)), where two S2m, one preceding and one following the acquisition date of the target S1 image are used. Furthermore, the TIM method was modified in order to produce results using only one S2m, either proceeding or following. The accuracy of the classification of the target S1 image was evaluated against the best fit alternative result used to produce the timely coinciding S2m; not previously used in the training process.

3 RESULTS AND DISCUSSION
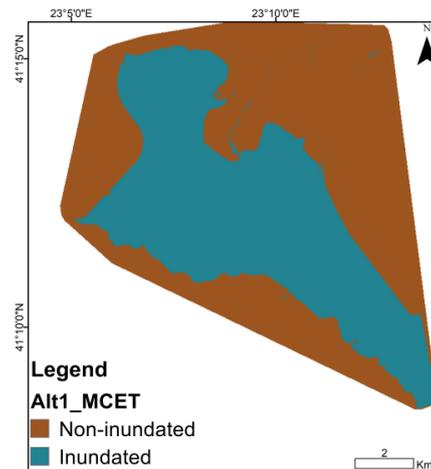
3.1 Inundation Maps Derived by Sentinel-2 Images

Accuracy assessment took into consideration all pixels present in the area with excellent results as indicated in Figure 1. In Table 1 is shown that the overall k ranged from 0.77 to 0.94, 'substantial' but mostly 'almost perfect' agreement according to Landis and Koch (1977) and overall accuracy ranged from 88.05 to 97.16%. Using Alt1, Band 11 (SWIR-1) as an initial threshold and applying MCET algorithm to find the final threshold, achieved the best classification performance.

Table 1: Overall accuracy assessment shows the use of the nine alternatives of local automatic thresholding in distinguishing between inundated and non-inundated pixels, averaged over all 22 images/ dates.
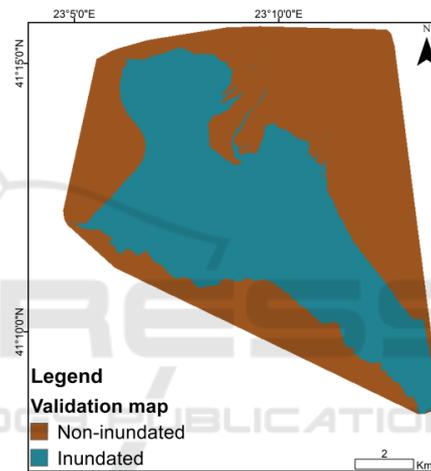
Alternatives	Overall Accuracy (%)	Overall kappa
Alt1 and MCET	97.16	0.94
Alt1 and Otsu's	96.82	0.93
Alt1 and average	97.08	0.94
Alt2 and MCET	91.32	0.83
Alt2 and Otsu's	89.77	0.79
Alt2 and average	91.03	0.82
Alt3 and MCET	89.06	0.79
Alt3 and Otsu's	88.05	0.77
Alt3 and average	90.22	0.81

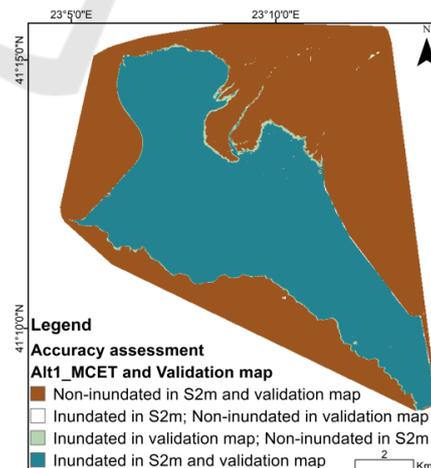## 3.2 Inundation Maps Derived Synergistically by Sentinel-2 and Sentinel-1 Images

For the two target dates examined with the TIM method, the S1m produced an overall accuracy over 99.71% in all cases, when compared with the S2m reference. The overall kappa values were all over 0.99 (Table 2).
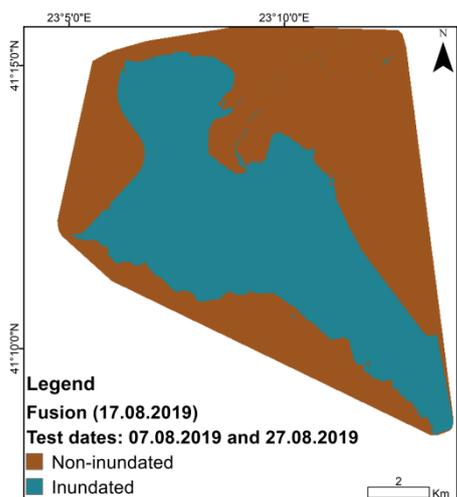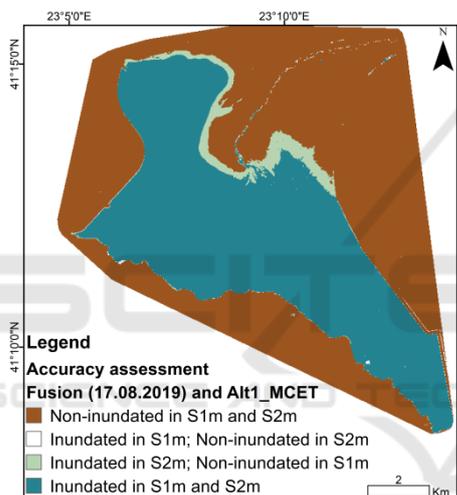

(a)

(b)

(c)

Figure 1: (a) Inundation map (example of 17 August 2019) derived Sentinel-2 image. (b) Validation layer. (c) Accuracy assessment (a) against (b).

(a)

(b)

Figure 2: (a) Inundation map (example: 17 August 2019) based on pixel centric classification using TIM (07 August 2019 and 27 August 2019). (b) Accuracy assessment on the inundation map S1m (17 August 2019) validated against the timely coinciding S2-derived inundation map (S2m) produced by best fit alternative. Training dates used: 07 August 2019 and 27 August 2019.

For the same target dates and by using the modified TIM method with reduced number of training S1 images (Table 3), 1 S2m was used to train the target S1 dates, and achieved lower accuracies than in Table 2, with overall accuracy of 83.11 to 99.78%, when compared to the reference S2m. The overall kappa values ranged from 0.62 to 0.98. It becomes clear that the method may be successfully applied with less S1 images and in various time intervals away from the target date; however, results are not as credible.

Table 2: Accuracy assessment of pixel-centric classification method done using TIM method applied to S1 images acquired on 08 March 2019 and 17 August 2019.

Target S1	Training dates		Accuracy (%)	kappa
	S2 images	S1 images		
08.03	28.02; 20.03	24.02; 02.03 20.03; 26.03	99.78	0.99
17.08	12.08; 22.08	11.08; 23.08	99.88	0.99
17.08	07.08; 27.08	05.08; 11.08 23.08; 29.08	99.77	0.99
17.08	02.08; 27.08	30.07; 05.08 23.08; 29.08	99.71	0.99

Table 3: Accuracy assessment of pixel-centric classification method done using the modified TIM method with reduced number of training S1 images acquired on 08 March 2019 and 17 August 2019.

Target S1	Training dates		Accuracy (%)	kappa
	S2 images	S1 images		
08.03	28.02	24.02; 02.03	99.78	0.98
08.03	25.03	20.03; 26.03	98.55	0.96
17.08	02.08	30.07; 05.08	83.11	0.62
17.08	07.08	05.08; 11.08	98.03	0.95
17.08	12.08	11.08	98.58	0.96
17.08	22.08	23.08	98.94	0.97
17.08	27.08	23.08; 29.08	98.26	0.95

3.3 Applicability of the Methods

The aim of this work was to assess the performance of unsupervised methods applied to Camargue and Doñana Biosphere Reverses, and its applicability for Kerkini Lake, an inland reservoir whose intense use across the years has suffered from a changing water extent due to the human pressures, and uncontrolled frequent extreme flooding events.

In relation with the use of the multispectral information, Kordelas et al. (2018, 2019) applied threshold techniques, which have been usually employed for radar images to quantify flood water extent (Grimaldi et al., 2016), on multispectral images and led to high mapping accuracy of the water extent in Kerkini Lake, as well. Minimum cross entropy thresholding (MCET) for the

estimation of the final threshold had consistent results with Camargue and Doñana marine coastal areas. The results from this work prove the efficacy of the methods in an inland water body and wetland. The alternative approaches Alt2 (MCET) and Alt3 (MCET) demonstrated also similarly good results as for Camargue and Doñana complete areas (Kordelas et al., 2019).

In relation with cases when unfavourable atmospheric conditions prevail, the sole use of radar images proves to fail achieving high accuracy due to backscatter confusion among landscape features, such as water with emergent vegetation, shadow effects, sandy areas, which may be classified either as belonging to the water or land class. The use of the pixel-centric classification has the ability to capture the pixel-related fluctuation of the backscatter across a time period, which in one case might mean inundation and in a neighbouring one no inundation. As a result the application of the pixel-centric classification with the use of one or two Sentinel-2 inundation maps up to a 30-day time interval from the targeted Sentinel-1 image, has achieved accurate results. The utilization of two Sentinel-2 inundation maps provided the best results in this study and is consistent with the results from its application at the Doñana Biosphere Reserve (Manakos et al., 2019).

The validation of the automation techniques provides consistent results for managing water use. In the case of Lake Kerkini the hydroperiods generated using the S2m and S1m throughout the years, revealed the intense reservoir use for flood control due to frequent extreme events, which assists in retaining a lower level of the lake. Seasonal patterns could be identified for various subareas within the delta and beyond.

4 CONCLUSIONS

This research contributes to the studies conducted by Kordelas et al. (2018, 2019) and Manakos et al. (2019) on the evaluation of the credibility and applicability of the developed methods for inundation mapping to other protected areas than coastal marine ones. It became evident that methods apply also at Lake Kerkini, a protected area and an artificially generated inland water body for flood mitigation in the plain of Serres, by achieving high accuracy.

High inundation mapping accuracy is achieved without the need for simultaneous ground truth data or user's intervention. Employing machine learning

through fusion of S-1 and S-2 data, allows the consistent delivery of products, overcoming the limitation of weather conditions and optical data. Further steps may utilize DEM or additional post-processing techniques to correct for hillshade or aspects. Additional index optimization could be applicable for areas with different types of vegetation. Automation of the process and minimum human interference further supports the implementation of the verified workflow as an effective service (even transformed to an online one) for Protected Areas management.

ACKNOWLEDGEMENTS

REFERENCES

Acharya, T. D., Subedi, A., & Lee, D. H. (2019). Evaluation of Machine Learning Algorithms for Surface Water Extraction in a Landsat 8 Scene of Nepal. *Sensors, 19*(12), 2769. https://doi.org/10.3390/s19122769

Cohen, S., Raney, A., Munasinghe, D., Loftis, D., Molthan, A., Bell, J., Rogers, L., Galantowicz, J., Brakenridge, G. R., Kettner, A. J., Huang, Y.-F., & Tsang, Y.-P. (2019). The Floodwater Depth Estimation Tool (FwDET v2.0) for Improved Remote Sensing Analysis of Coastal Flooding. *Natural Hazards and Earth System Sciences Discussions, 2017*, 1–15. https://doi.org/10.5194/nhess-2019-78

Congalton, R. G., & Green, K. (2009). Assessing the Accuracy of Remotely Sensed Data: Principles and Practices. In *Psychology Applied to Work: An Introduction to Industrial and Organizational Psychology, Tenth Edition Paul* (Second, Vol. 53, Issue 9). CRC Press Taylor & Francis group.

Du, Y., Zhang, Y., Ling, F., Wang, Q., Li, W., & Li, X. (2016). Water Bodies' Mapping from Sentinel-2 Imagery with Modified Normalized Difference Water Index at 10-m Spatial Resolution Produced by Sharpening the SWIR Band. *Remote Sensing, 8*(4), 354. https://doi.org/10.3390/rs8040354

Feng, Q., Gong, J., Liu, J., & Li, Y. (2015). Flood Mapping Based on Multiple Endmember Spectral Mixture Analysis and Random Forest Classifier—The Case of Yuyao, China. *Remote Sensing, 7*(9), 12539–12562. https://doi.org/10.3390/rs70912539

Feyisa, G. L., Meilby, H., Fensholt, R., & Proud, S. R. (2014). Automated Water Extraction Index: A new technique for surface water mapping using Landsat

imagery. *Remote Sensing of Environment, 140*, 23–35. https://doi.org/10.1016/j.rse.2013.08.029

Filipponi, F. (2019). Sentinel-1 GRD Preprocessing Workflow. *Proceedings, 18*(11), 1–4. https://doi.org/10.3390/ECRS-3-06201

Finlayson, C. M., & D'Cruz, R. (2010). Inland Water Systems. In *Ecosystems and Human Well-being: Current State and Trends* (Vol. 1, Issue January, pp. 551–583). http://www.millenniumassessment.org/en/Condition.html

Gerakes, P. A. (Ed.). (1989). Conservation and Management of Greek Wetlands. In *Proceedings of a Workshop on Greek Wetlands* (p. 493). IUCN, 1992.

Grimaldi, S., Li, Y., Pauwels, V. R. N., & Walker, J. P. (2016). Remote Sensing-Derived Water Extent and Level to Constrain Hydraulic Flood Forecasting Models: Opportunities and Challenges. *Surveys in Geophysics, 37*(5), 977–1034. https://doi.org/10.1007/s10712-016-9378-y

Guo, M., Li, J., Sheng, C., Xu, J., & Wu, L. (2017). A Review of Wetland Remote Sensing. *Sensors, 17*(4), 777. https://doi.org/10.3390/s17040777

Ko, B., Kim, H., & Nam, J. (2015). Classification of Potential Water Bodies Using Landsat 8 OLI and a Combination of Two Boosted Random Forest Classifiers. *Sensors, 15*(6), 13763–13777. https://doi.org/10.3390/s150613763

Kordelas, G., Manakos, I., Aragonés, D., Díaz-Delgado, R., & Bustamante, J. (2018). Fast and Automatic Data-Driven Thresholding for Inundation Mapping with Sentinel-2 Data. *Remote Sensing, 10*(6), 910. https://doi.org/10.3390/rs10060910

Kordelas, G., Manakos, I., Lefebvre, G., & Poulin, B. (2019). Automatic Inundation Mapping Using Sentinel-2 Data Applicable to Both Camargue and Doñana Biosphere Reserves. *Remote Sensing, 11*(19), 20. https://doi.org/10.3390/rs11192251

Landis, J., & Koch, G. (1977). The Measurement of Observer Agreement for Categorical Data. *Biometrics, 33*(1), 159-174. https://doi.org/10.2307/2529310

Main-Knorn, M., Pflug, B., Louis, J., Debaecker, V., Müller-Wilm, U., & Gascon, F. (2017). Sen2Cor for Sentinel-2. In L. Bruzzone, F. Bovolo, & J. A. Benediktsson (Eds.), *Image and Signal Processing for Remote Sensing XXIII* (p. 3). SPIE. https://doi.org/10.1117/12.2278218

Manakos, I., Kordelas, G. A., & Marini, K. (2019). Fusion of Sentinel-1 data with Sentinel-2 products to overcome non-favourable atmospheric conditions for the delineation of inundation maps. *European Journal of Remote Sensing*, 1–14. https://doi.org/10.1080/22797254.2019.1596757

Marti-Cardona, B., Dolz-Ripolles, J., & Lopez-Martinez, C. (2013). Wetland inundation monitoring by the synergistic use of ENVISAT/ASAR imagery and ancilliary spatial data. *Remote Sensing of Environment, 139*(June 2018), 171–184. https://doi.org/10.1016/j.rse.2013.07.028

McFeeters, S. K. (1996). The use of the Normalized Difference Water Index (NDWI) in the delineation of open water features. *International Journal of Remote Sensing, 17*(7), 1425–1432. https://doi.org/10.1080/01431169608948714

Millennium Ecosystem Assessment. (2005). *Ecosystems and Human Well-being: Synthesis*. Island Press.

Nandi, I., Srivastava, P. K., & Shah, K. (2017). Floodplain Mapping through Support Vector Machine and Optical/Infrared Images from Landsat 8 OLI/TIRS Sensors: Case Study from Varanasi. *Water Resources Management, 31*(4), 1157–1171. https://doi.org/10.1007/s11269-017-1568-y

Ovakoglou, G., Alexandridis, T. K., Crisman, T. L., Skoulikaris, C., & Vergos, G. S. (2016). Use of MODIS satellite images for detailed lake morphometry: Application to basins with large water level fluctuations. *International Journal of Applied Earth Observation and Geoinformation, 51*, 37–46. https://doi.org/10.1016/j.jag.2016.04.007

Psilovikos, A., & Margoni, S. (2010). An empirical model of sediment deposition processes in Lake Kerkini, Central Macedonia Greece. *Environmental Monitoring and Assessment, 164*(1–4), 573–592. https://doi.org/10.1007/s10661-009-0914-9

Rokni, K., Ahmad, A., Selamat, A., & Hazini, S. (2014). Water Feature Extraction and Change Detection Using Multitemporal Landsat Imagery. *Remote Sensing, 6*(5), 4173–4189. https://doi.org/10.3390/rs6054173

Sarp, G., & Ozcelik, M. (2017). Water body extraction and change detection using time series: A case study of Lake Burdur, Turkey. *Journal of Taibah University for Science, 11*(3), 381–391. https://doi.org/10.1016/j.jtusci.2016.04.005

Skakun, S. (2010). A neural network approach to flood mapping using satellite imagery. *Computing and Informatics, 29*, 1013–1024.

Thenkabail, P. S. (2015). Remotely Sensed Data Characterization, Classification, and Accuracies. In *Remotely Sensed Data Characterization, Classification, and Accuracies* (Vol. 1). CRC Press. https://doi.org/10.1201/b19294

Tsolakidis, I., & Vafiadis, M. (2019). Comparison of Hydrographic Survey and Satellite Bathymetry in Monitoring Kerkini Reservoir Storage. *Environmental Processes, 6*(4), 1031–1049. https://doi.org/10.1007/s40710-019-00394-7

Whitten, I. H., Frank, E., & Hall, M. A. (2011). *Data Mining: Practical Machine Learning Tools and Techniques* (Third). Elsevier. https://doi.org/10.1016/C2009-0-19715-5

Xu, H. (2006). Modification of normalised difference water index (NDWI) to enhance open water features in remotely sensed imagery. International Journal of *Remote Sensing, 27*(14), 3025–3033. https://doi.org/10.1080/01431160600589179

Yousefi, P., Jalab, H. A., W. Ibrahim, R., Mohd Noor, N. F., Ayub, M. N., & Gani, A. (2018). Water-Body Segmentation in Satellite Imagery Applying Modified Kernel K-Means. *Malaysian Journal of Computer Science, 31*(2), 143–154. https://doi.org/10.22452/mjcs.vol31no2.4

Zhang, F., Li, J., Zhang, B., Shen, Q., Ye, H., Wang, S., & Lu, Z. (2018). A simple automated dynamic threshold extraction method for the classification of large water bodies from landsat-8 OLI water index images. *International Journal of Remote Sensing*, *39*(11), 3429–3451. https://doi.org/10.1080/01431161.2018.14 44292